ROYAL SOCIETY
OF CHEMISTRY

PAPER

Check for updates

Hydrazine functionalized probes for chromogenic and fluorescent ratiometric sensing of pH and F⁻: experimental and DFT studies†

Additi Roy Chowdhury,[a,b] Amita Mondal,[a,c] Biswajit Gopal Roy,[d] Jagadeesh C. Bose K,[e] Sudit Mukhopadhyay[e] and Priyabrata Banerjee ✦[a,b]

Two novel hydrazine based sensors, **BPPIH** (N^1,N^3-bis(perfluorophenyl)isophthalohydrazide) and **BPBIH** ($N^{1'},N^{3'}$-bis(perfluorobenzylidene)isophthalohydrazide), are presented here. **BPPIH** is found to be a highly sensitive pH sensor in the pH range 5.0 to 10.0 in a DMSO−water solvent mixture with a pK_a value of 9.22. Interesting optical responses have been observed for **BPPIH** in the above mentioned pH range. **BPBIH** on the other hand turns out to be a less effective pH sensor in the above mentioned pH range. The increase in fluorescence intensity at a lower pH for **BPPIH** was explained by using density functional theory. The ability of **BPPIH** to monitor the pH changes inside cancer cells is a useful application of the sensor as a functional material. In addition fluoride (F⁻) selectivity studies of these two chemosensors have been performed and show that between them, **BPBIH** shows greater selectivity towards F⁻. The interaction energy calculated from the DFT-D3 supports the experimental findings. The pH sensor (**BPPIH**) can be further interfaced with suitable circuitry interfaced with desired programming for ease of access and enhancement of practical applications.

Introduction

In recent times the development of chromogenic and fluorogenic chemosensors having a wide range of analytical applications is of prime importance.[1] In this context, the development of sensors for both pH and biologically important anions like F⁻ is of enormous significance.[1] Accordingly two newly made hydrazine based fluorescent chemosensors,[1] **BPPIH** and **BPBIH**, are reported here and their applicability as a pH sensor and a low level F⁻ sensor has been

studied. The sensor **BPPIH** is an amide based organic material and the other one, *i.e.*, **BPBIH**, has both amide and azomethine linkages within its molecular framework. The pentafluorophenyl part in both chemosensors takes the leading role in tuning the acidity of the NH hydrogens thus increasing their hydrogen donating ability. The pentafluoro part also serves as the fluorophore part where electron transfer takes place from the adjacent NH groups. After the synthesis of **BPPIH** and **BPBIH** a complete set of experiments were performed in order to establish them as suitable sensors for pH and F⁻.

First and foremost we did a case study by varying the solvents for these molecules. Since in general the solvent molecules have some influence on the bonding and thereafter influence the interaction between the sensor and analyte,[2] a study to analyse the effect of the solvent on the sensors is executed to get an idea of the appropriate solvent in which their sensing studies have to be performed.

It is well known that pH plays a vital role in physiological processes. The normal pH of cells inside the human body in general varies between 6.8 and 7.4.[3] Variation in pH (higher or lower than the normal pH) often results in abnormal functioning of cells. Typically cancer cells are associated with noticeably altered pH in comparison to normal cells.[4] From this perspective it becomes very important to develop low cost efficient pH sensors for monitoring intracellular activities.

[a]*Surface Engineering & Tribology Group, CSIR-Central Mechanical Engineering Research Institute, Mahatma Gandhi Avenue, Durgapur 713209, India. E-mail: pr_banerjee@cmeri.res.in, priyabrata_banerjee@yahoo.co.in; http://www.cmeri.res.in and www.priyabratabanerjee.in; Fax: +91 343 2546 745; Tel: +91 343 6452220*
[b]*Academy of Scientific and Innovative Research, CSIR-Central Mechanical Engineering Research Institute (CMERI) Campus, Mahatma Gandhi Avenue, Durgapur 713209, West Bengal, India*
[c]*Department of Chemistry, National Institute of Technology, M. G. Avenue, Durgapur, 713209, India*
[d]*Department of Chemistry, Sikkim University, Gangtok-737102, Sikkim, India*
[e]*Department of Biotechnology, National Institute of Technology, M. G. Avenue, Durgapur, 713209, India*
†Electronic supplementary information (ESI) available: UV-Vis, ESI-MS, ¹H-NMR and FT-IR of **BPPIH** and **BPBIH**. Crystallographic data of the structure **BPPIH**. CCDC 1442033. For ESI and crystallographic data in CIF or other electronic format see DOI: 10.1039/c7pp00246g

In view of the above and as a part of our ongoing research on cancer cells[5] several experiments on **BPPIH** and **BPBIH** have been performed to judge their usefulness as promising pH sensors for cancer cells, and interestingly it is found that **BPPIH** has the potential for pH monitoring inside cancer (HeLa) cells. Density Functional Theoretical (DFT) and modern DFT-D3 studies[6] are well examined to support the experimental outcomes.

Finally both **BPPIH** and **BPBIH** show affinity towards F^-. **BPPIH** turns out to be a non-ratiometric F^- sensor[7] whereas **BPBIH** shows a ratiometric[8] approach towards absorbance and emission profiles with F^-. Interestingly **BPPIH** displays a greater binding constant value with F^- than **BPBIH** whereas the limit of detection is in just the reverse order.

Experimental

Materials

All starting materials (chemical reagents, solvents) were commercially available and of analytical grade. Solvents like acetonitrile (ACN), dichloromethane, methanol, and ether were distilled and dried prior to use. All tetrabutyl ammonium salts of anions like fluoride (hydrate), chloride, nitrate, bromide, hydrogen sulfate, acetate and phosphate were purchased from Sigma Aldrich chemical company and used as received. DMSO was of spectroscopic grade and purchased from Merck India Pvt. Ltd and used without any further purification.

Apparatus

The infrared spectra were recorded in a PerkinElmer FT-IR Spectrum 100 spectrophotometer. The mass spectra were obtained by using an Advion's CMS Expression serial number: 3013-0140 compact mass spectrometer. ^{1}H-NMR was recorded with a Bruker AV-400 spectrometer. UV-Vis spectra were recorded with a CARY60 spectrophotometer. Fluorescence experiments were done by using a PerkinElmer LS-45 spectrometer.

Synthesis

[N^1,N^3-Bis(perfluorophenyl)isophthalohydrazide] (BPPIH) (Scheme S1, ESI†). Isophthaloyl dichloride (102 mg, 0.5 mM) in 1.5 ml of dry dichloromethane (DCM) was added to a mixture of triethylamine (~0.15 ml), pentafluorophenyl hydrazine 1 mM (0.19 g) and 100 ml of dry DCM over a period of 5 minutes. After continuous stirring for 24 h a white precipitate appeared which was filtered. The solid residue obtained was purified by repeated recrystallization from DCM. Single crystals are obtained from a solution of acetonitrile and dichloromethane mixture after five days. The compound was characterized by elemental analysis (CHN), IR, ESI-MS, ^{1}H-NMR along with single crystal X-ray analysis (Fig. S1, S3, S5, S7, S8a, S8b, S9 and Tables S1–S4, ESI†). CHN anal. calcd for $C_{22}H_{11}F_{10}N_5O_2$: C: 50.19%; H: 2.09%; N: 13.3%; found. C: 50.4%; H: 2.0%; N: 12.8%. Yield: 212 g, 80.6%; m.p. 202 °C; (m/z) calcd 526 for $C_{22}H_{11}F_{10}N_5O_2$: found 527 [**BPPIH** + H^+]: ^{1}H-NMR (300 MHz, DMSO-d^6, Me$_4$Si) δ = 10.890 (s, 2H), 8.298 (s, 2H), 8.298 (s, 1H), 8.033 (d, 2H), 7.663 (s, 1H).

[N^1,N^3-Bis(perfluorobenzylidene)isophthalohydrazide] (BPBIH) (Scheme S2, ESI†). Hydrazine hydrate (80%) 0.06 mM was dissolved in dry DCM. This solution was added to a solution containing isophthaloyl chloride (5 mM) in DCM in the presence of 0.5 ml triethylamine. The mixture was stirred for 1 hour at room temperature (rt) under N_2 atmosphere. The solvent evaporated and a yellowish colored gummy compound was obtained which was washed with ethanol thrice in small fractions. The purified dried product was white. Then 0.5 mM of the white product was dissolved in methanol and to it 1 mM of (0.19 g) pentafluorobenzaldehyde was added with stirring. The stirring was continued for the next 8 hours. Finally the solvent was evaporated and the product was collected. The compound was characterized by elemental analysis (CHN), IR, ESI-MS, ^{1}H-NMR along with single crystal X-ray analysis (Fig. S2, S4, S6 and S10, ESI†). CHN anal. calcd for $C_{22}H_{11}F_{10}N_5O_2$: C: 48%; H: 2%; N: 12.72%; found; C: 47.9%; H: 1.8%; N: 12.2%. Yield: 190 g, 69%; m.p. 202 °C; (m/z) calcd 550 for $C_{22}H_{11}F_{10}N_5O_2$: found 549 [**BPBIH** − H^+]: ^{1}H-NMR (400 MHz, DMSO-d^6, Me$_4$Si) δ = 12.5 (s, 2H), 10.8 (s, 2H), 9–8 (5Ar-Hs).

Computational details

DFT calculations were performed using the ORCA program package[9a] and Turbomole (v7.0).[9b] Furthermore, investigation of the different non-covalent interactions was carried out with Grimme's third generation dispersion (D3)[9c] corrections with inclusion of Becke–Johnson (BJ)[9d] damping parameter during computational experimentation. The geometry optimizations were carried out at the B3LYP level[10–12] of DFT. The all-electron Gaussian basis sets were those reported by the Ahlrichs group.[13,14] Triple-ξ quality basis sets (TZVP) with one set of polarization functions were used for fluorine, nitrogen, and oxygen like atoms.[14] The carbon and hydrogen atoms were described by smaller polarized split-valence SV(P) basis sets and double-ξ quality in the valence region with a polarizing set of d-functions on the non-hydrogen atoms.[13] The self-consistent field (SCF) calculations were tightly converged [1×10^{-8} E_h (Hartree energy) in energy, 1×10^{-7} E_h in the density change, and 1×10^{-7} in the maximum element of the Direct Inversion in Iterative Subspace (DIIS) error vector]. The geometries were considered to be converged after the energy change was less than 5×10^{-6} E_h, the gradient norm and maximum gradient element were smaller than 1×10^{-4} E_h per Bohr and 3×10^{-4} E_h per Bohr, respectively, and the root-mean square and maximum displacements of the atoms were smaller than 2×10^{-3} Bohr and 4×10^{-3} Bohr, respectively. The corresponding orbitals[15] and density plots were subsequently generated using the program Molekel (v 4.3).

Background equation used in DFT. The DFT energy expressed as a functional of the molecular electron density $\rho(r)$ is shown in eqn (1):

$$E_{DFT}[\rho] = T[\rho] + V_{ne}[\rho] + J[\rho] + E_x[\rho] + E_c[\rho] + V_{nuc} \qquad (1)$$

where $T[\rho]$ is the kinetic energy, $J[\rho]$ is the classical Coulomb repulsion of the electrons, $V_{ne}[\rho]$ is the nuclei–electron inter-

This journal is © The Royal Society of Chemistry and Owner Societies 2017

Photochem. Photobiol. Sci., 2017, **16**, 1654–1663 | **1655**

action, $E_x[\rho]$ and $E_c[\rho]$ are the exchange and correlation energy functional, and V_{nuc} is the nuclear repulsion energy.

Calculation of interaction energy. The basic approach for evaluating interaction energy is to calculate the difference between the energies of isolated objects and that of their assembly. In the case of two objects, A and B, the interaction energy can be written as in eqn (2):

$$\Delta E_{int} = E_{(A,B)} - [E_{(A)} + E_{(B)}] \qquad (2)$$

where $E_{(A)}$ and $E_{(B)}$ are the energies of the monomers A (**BPPIH/BPBIH**) and B (NMe$_4$F) and $E_{(A,B)}$ is the energy of their interacting assembly.

X-ray crystallography

A Bruker-Nonius Kappa CCD diffractometer equipped with a Mo-target rotating-anode X-ray source and a graphite monochromator (Mo KR, $\lambda = 0.71073$ Å) was used throughout. Final cell constants were obtained from least-squares fits of all measured reflections. Intensity data were corrected for absorption using the intensities of redundant reflections. The structures were readily solved by Patterson methods and subsequent difference Fourier techniques. The Bruker ShelXTL[16] software package was used for the solution, refinement and artwork of the structures. All non-hydrogen atoms were anisotropically refined and hydrogen atoms were placed at calculated positions and refined as riding atoms with isotropic displacement parameters.

Results and discussion

The crystal structure (50% ellipsoid) of **BPPIH** is shown in Fig. 1. The single crystal of **BPPIH** is crystallized in the space group $P\bar{1}$ (no. 2). The crystals are obtained from an acetonitrile/toluene solution mixture (*vide supra* Experimental section). **BPPIH** is nonplanar. The C–N bond distance of C9–N8 is 1.35 Å and that of C6–N7 is 1.40 Å, which are less than the C–N distances generally in the range of 1.47 Å (ref. 17). The C–N distances of the other arm *i.e.* C16–N17: 1.35 Å and C19–N18: 1.41 Å are different. The N–N distances 1.40 Å and 1.41 Å, respectively, are slightly less than the N–N bond distances in hydrazine. The molecule shows atropisomerism because of
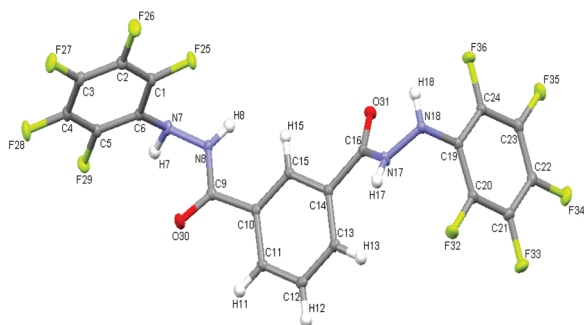
hindered rotation about the N–N single bond. The crystal structure is obtained in the *trans* form as this form is more stable than the *cis* form. The C9–N8–N7 angle 119.87°, N8–N7–C6 angle 115.82°, C16–N17–N18 angle 120.2° and N17–N18–C19 112.09° of both the sides suggest disparity and lack of symmetry in the molecule. In a unit cell, two **BPPIH** molecules are co-crystallized and form a closely packed structure along the crystallographic *a* axis. The structure also shows extensive intermolecular H-bonding between acidic N–H protons with an electronegative oxygen (O) atom (NH···O) making a supramolecular 2D-network with a zig-zag configuration (Fig. S8a, ESI†).

Prior to an analysis of the response of the sensors in wide pH range, their configuration has to be well explored. From X-ray crystallography the structural property and configuration of **BPPIH** have been well understood. In the case of **BPBIH**, the poor crystal quality resulted in failure in collecting its data. In order to understand the configuration of **BPBIH**, it is necessary to optimize its geometry with a hybrid functional like B3LYP. Therefore, with the ORCA program package and B3LYP function the geometry was optimized. Initially, **BPPIH** was optimized where the coordinates were directly taken from the crystallographic information file (CIF). After optimization, it was observed that the geometry, along with the other parameters of **BPPIH**, was in good agreement with the experimental results (*vide supra*, CIF of **BPPIH**). Calculated C–O, C–C and C–N bond distances are within the permissible experimental error limit of ±0.02 Å. After obtaining reliable and reproducible results from ORCA supported DFT calculation with atomic coordinates of **BPPIH** (see Table S5, ESI†), a similar calculation was performed with **BPBIH**. During the calculation of **BPBIH**, concerning atomic coordinates, for the sake of clarification, except for introducing the two sp^2 hybridized carbon atoms, the rest of the hypothetical atom coordinates of **BPBIH** were taken from crystallographically characterized **BPPIH** molecules (Table S6, ESI†).[6c] After optimization of the geometry its configuration has been explored. In Fig. 2, HOMO, LUMO along with ΔE has been plotted.

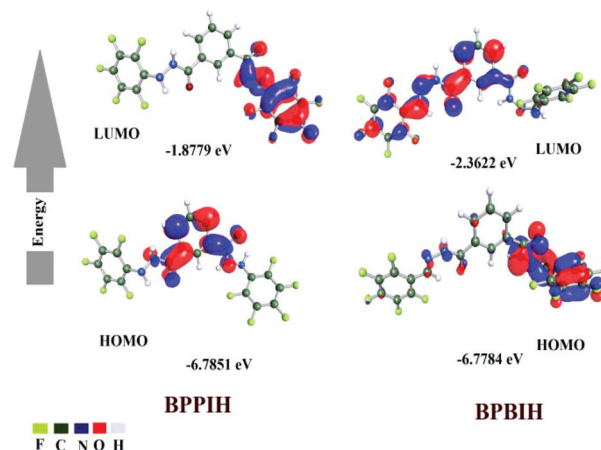**Fig. 1** ORTEP and atom numbering scheme of **BPPIH**.

Fig. 2 The frontier molecular orbitals of **BPPIH** and **BPBIH**.

Theoretical calculations

Theoretical calculation (Fig. 2) has shown that **BPPIH** has a larger HOMO–LUMO energy gap (4.9 eV) than that of **BPBIH** (4.41 eV). The larger the HOMO–LUMO energy gap, the less is the possibility of solvent molecules deactivating the energy.[18] Thus the emission intensity of **BPPIH** (in DMSO solvent) is found to be much higher than that of **BPBIH** (Fig. S16 and S17, ESI†).

Absorption spectra

The absorption profile of **BPPIH** (10^{-4} M) in DMSO shows a broad absorption band at 265 nm (Fig. S9, ESI†). However, in DMSO with varying concentration as shown in Fig. S11, ESI† the absorption peak is slowly red shifted from 260 to 270 nm with increasing concentration from 10^{-5} M to 10^{-3} M. The plot of λ_{max} vs. concentration profile is shown in Fig. S12, ESI.† The increase in concentration causes the stacking and aggregation of more and more numbers of **BPPIH** molecules, which in turn shifts the λ_{max} towards higher wavelengths with better absorption profile.[19] The UV absorption of **BPPIH** in DMSO is in a region of 260–270 nm where the solvent is not transparent. However, when the absorption profile of **BPPIH** in MeOH, ACN and EtOH is seen, it is found that an absorption maxima at 265 nm exists which suggests that a real peak exists there. The peak at 265 nm corresponds to the n–π* transition of the carbonyl group. In other less polar solvents like methanol, ethanol and acetonitrile, **BPPIH** (10^{-5} M) shows one sharp peak at 225 nm which is the π–π* transition and the broader shoulder peak observed at 275 nm, is the n–π* transition (Fig. S14, ESI†). There was not much shifting of n–π* and π–π* responses with change of solvent polarity. The relative absorbance intensity for the same concentration of the **BPPIH** sensor is the highest in methanol followed by ethanol and acetonitrile. However the scenario is different in the excited state and we observe that polar solvents had a greater bathochromic effect on **BPPIH**. This indicates the existence of ICT in the excited state of the molecule.[20] In the case of **BPBIH** the absorption maxima in DMSO is at 300 nm (Fig. S10, ESI†). The peak positions remain unaltered (λ_{max} remains at same position) even after varying the concentration of the sensor (Fig. S13, ESI†). These results suggest less interaction (H-bonding) of the molecule with the solvent.[21] In comparatively less polar solvents, e.g. methanol, ethanol and in acetonitrile two peaks are observed viz. 210 nm (π–π*) and 300 nm (n–π*) (Fig. S15, ESI†).

Excitation and emission spectra

In **BPPIH** the acidic hydrazine protons (i.e. NH protons) create H-bonding with the electronegative "O" centre of the amide moiety of the **BPPIH** molecule. Moreover it is also found from single crystal XRD that the co-crystallized solvent, here acetonitrile, with its N side is also H-bonded with the hydrazine NH protons of one of the two side arms of the **BPPIH** sensor molecule (Fig. S8b, ESI†). As a result, the system as a whole becomes highly rigid. The restricted rotation about the N–N

single bond (atropisomerism) due to sterically encumbered units in the tail part of the **BPPIH** molecule makes it more rigid as well. It is a well established fact that rigid fluorophores are more fluorescent.[22] The high rigidity of **BPPIH** is thus reflected from the high emission intensity in the system in the polar DMSO solvent, which reduces with a decrease in polarity for ACN and MeOH (Fig. S16, ESI†). **BPBIH** on the other hand shows much less intensity where such intermolecular H-bonding is relatively less, making the molecule more flexible. The low emission intensity for **BPBIH** in DMSO is observed in Fig. S17, ESI.† The stokes shift values for **BPBIH** are greater than those for **BPPIH**, which also indicates greater flexibility and less rigidity in the **BPBIH** molecule. Table 1 summarizes the optical properties of the two sensors. The quantum yield for **BPPIH** is 0.3768 and for **BPBIH** the quantum yield is 0.01002.

pH study

In the first stage, during the addition of a low concentration (10^{-3} M) of base in **BPPIH**, the initial base peak at 260 nm is gradually decreased; new peaks at 270 nm and 340 nm developed with an isosbestic point at 265 nm (Fig. 3a). Visually the color turned from colorless to yellow (Fig. 3c). The pH is monitored to change from 5 to 8. On the addition of a more concentrated NaOH solution a few more interesting results are found. The initial **BPPIH** response at 270 nm along with the response

Table 1 Optical properties of **BPPIH** and **BPBIH**

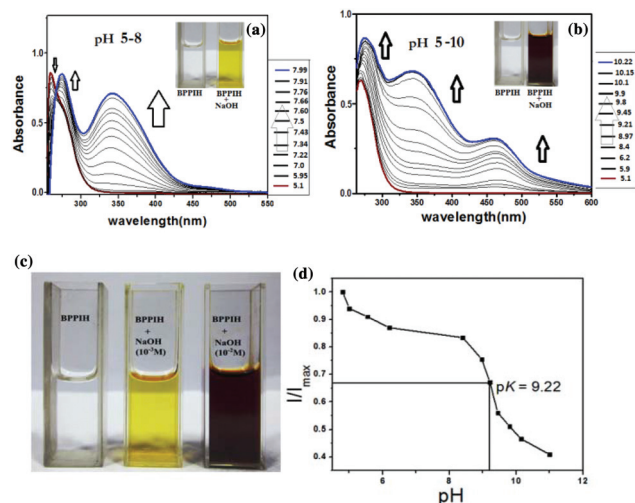| Sensors	λ_{abs} (max/nm)	λ_{em} (max/nm)	I_{max} (approx.)	$\log \varepsilon$
BPPIH	265	370	250	4.87
BPBIH	300	380	20	4.88

Fig. 3 (a) Titration of **BPPIH** (1×10^{-5} M) in DMSO/H_2O medium with low concentration NaOH solution (10^{-3} M): pH is changing from 5−8; (b) titration of **BPPIH** (1×10^{-5} M) in DMSO/H_2O medium with high concentration of NaOH (10^{-2} M): pH is changing from 5−10; (c) color changes of **BPPIH** from yellow to red on increasing the concentration of base; (d) the ratio of emission intensity as a function of pH.

This journal is © The Royal Society of Chemistry and Owner Societies 2017

Photochem. Photobiol. Sci., 2017, **16**, 1654–1663 | **1657**

at 340 nm increased in intensity. However, in addition to that a new peak at 465 nm appeared to rise (Fig. 3b). Finally, the color turns from colorless to blood red (Fig. 3c) when the pH changes from 5.0 to 10.0. The generation of such interesting colors may be due to the rupture of existing extensive intermolecular H-bonding within the molecular scaffold and formation of new H-bonding interactions with added base (OH⁻ ions) and base mediated ligand to ligand charge transfer in the supramolecular network. The H-bonding is also supported by the ¹H-NMR titrations of NaOH with **BPPIH** in DMSO-d₆ (Fig. S22, ESI†) where no shifting of protons occurs.[1c] Thus the system shows pH sensing based on H-bonding interactions.[23] In the pH range 5.0–10.0 the emission intensity of **BPPIH** is not only drastically reduced (Fig. S18, ESI†) but the peak position is also red shifted from 370 nm to 435 nm. The disruption of the intermolecular H-bonds[24] and increase of negative charge density in the system make PET followed by ICT feasible and favourable. The pK_a is found to be 9.22 (Fig. 3d). The UV-Vis changes of **BPPIH** after base treatment in MeOH are shown in Fig. S20, ESI† which are not as promising as the results seen in DMSO, substantiating the importance of the solvent in sensing studies. In a highly acidic medium (pH = 1) the emission intensity is found to be enhanced (Fig. S19, ESI†), although in UV and ¹H-NMR titration studies no observable changes of **BPPIH** were noticed when titrated with the same solution of HCl (at pH = 1) (Fig. S21 and S23, ESI†). Since **BPPIH** is considered as a PET induced pH sensor, the fluorescence enhancement with protonation of NH moieties can be well explained by the theory of PET blocking. Molecular and electronic level *ab initio* calculations of the neutral and protonated form are performed to explain the blocking of PET at lower pH in **BPPIH** using the ORCA program package (Fig. 4, Tables S7–S10, ESI†). The geo-

metry optimizations are carried out at the B3LYP level of DFT. In Fig. 4 it is seen that the HOMO of the neutral isophthalohydrazide moiety on the left of the pentafluorophenyl part is higher in energy (−7.19 eV) than the HOMO of the pentafluoro part (−7.33 eV). As a result, reductive PET occurs and due to this self decay process there is occurrence of fluorescence quenching.

On the other hand after protonation as shown on the right side of the pentafluoro moiety there is reduction in the energy of the HOMO (−7.4468 eV) of isophthalohydrazide moiety which prevents PET and as a result fluorescence enhancement occurs. The figure (Fig. 4) on the extreme right shows reduction in energy with further protonation. In the case of **BPBIH** low emission intensity, less solubility in aqueous medium and insignificant noisy spectral responses with solutions of NaOH and HCl in water (Fig. S24–S27, ESI†) make this molecule an ineffective pH sensor in the above mentioned pH range.

The pH sensitivity of **BPPIH** covering such a wide range (pH 5–10), including the physiological pH range, creates a huge biological significance of the molecule and makes it a potential candidate as a pH sensor inside living human cells although the pK_a is 9.22. Generally the pK_a of pH sensors for *in vitro* application lies in the range of 4–8.[25] However, there are reports in the literature of sensors with a pK_a value less than 4 and above 8 detecting intracellular pH.[26]

pH changes inside living cells

This fluorescence study was performed with a Zeiss observer Z1 microscope. At a lower pH (*i.e.* under acidic conditions) all the cells showed increase in luminescence whereas at a higher pH a quenching in luminescence by the cells is observed. In Fig. 5 the decrease of emission fluorescence intensity with an increase in pH from 6– to 8 is reported. The cells were cultured in PBS buffer and **BPPIH** in DMSO is applied within the cells. HeLa cells (human cervical cancer) are used in this study for showing the fluorescence response of **BPPIH** inside cancer cells under different conditions. The cells are cultured in DMEM (Dulbecco's Modified Eagle's Medium) with 10% FBS (fetal bovine serum) and appropriate penicillin and streptomycin antibiotics. The cells are maintained under three different pH conditions like acidic (pH 6.0), neutral (pH 7.0) and alkaline (pH 8.0) conditions before treatment with **BPPIH**. Then all the cells are treated with **BPPIH** (∼1 × 10⁻⁶ M) and allowed to be uptaken in order to exhibit fluorescence. The remaining Experimental section is provided in the ESI.†

Multiple processing steps were allowed to culture the cells for fluorescence microscopy. Fluorescence microscopy of live cells uses either genetically encoded fluorescent protein like GFP, mCherry, YFP, RFP, *etc.* or cell membrane-permeable, non-toxic fluorescent stains. Fluorescence microscopy of fixed cells uses a fixative agent that renders the cells dead, but maintains cellular structure, allowing the use of specific antibodies and dyes to investigate cell morphology and structure. Appropriate sample preparation is necessary to ensure that high quality images are captured. Here we describe a number
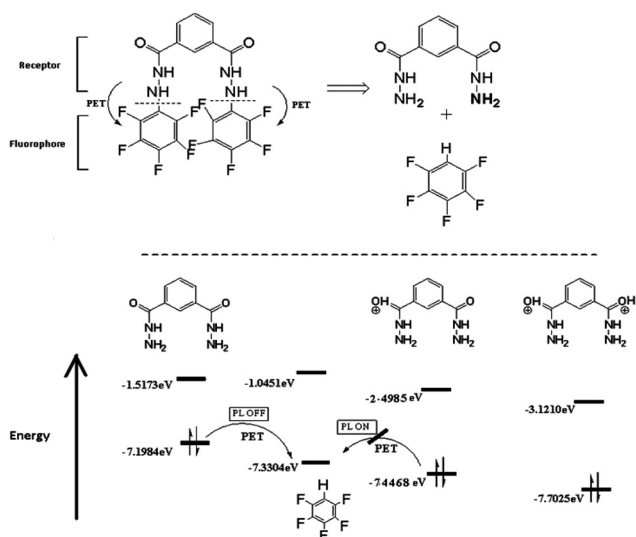

Fig. 4 Proposed photoinduced electron transfer (PET) mechanism between the isophthalohydrazide moiety and pentafluoro phenyl unit of **BPPIH** in protonated and neutral forms, respectively.
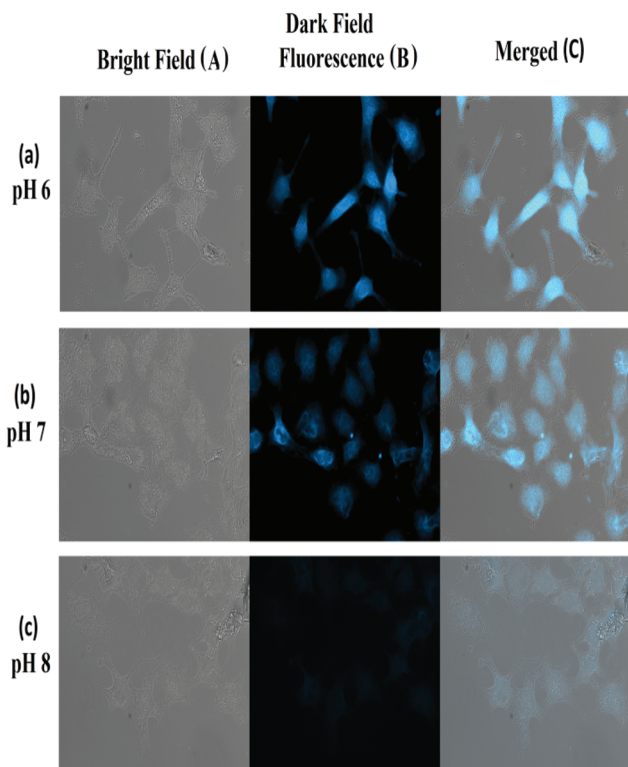
Fig. 5 The microscopic live cell imaging study (pH = 6/7/8 respectively) of the different HeLa cells maintained under different pH conditions treated with **BPPIH** taken in a bright field (a), dark fluorescence background (b) and merged image of both the backgrounds (c) to show the pattern of luminescence exhibited by all the cells in the microscopic field. (a) At acidic pH the cells were exhibiting remarkably higher fluorescence when compared to the cells maintained under neutral (b) and alkaline conditions (c). The merged image pattern suggests that the luminescence was observed in all the cells and its intensity depends on pH of the cell growth environment.

of concepts and considerations regarding the sample preparation process that can assist with automated digital fluorescence microscopy of fixed cells. Cell fixation by using cross linking agents does not reduce the cell membrane structure and rigidity. However, formaldehyde fixation enables the cells to be permeabilized to allow the **BPPIH** compound access the interior of cells. The size and ionic nature of the **BPPIH** compound prevent them from gaining access without membrane disruption. A mild detergent was used that generates large enough pores for the internalization of the **BPPIH** compound by passing through without completely dissolving the plasma membrane. Triton X-100 is the most commonly used permeabilization agent for immunofluorescent staining. This detergent efficiently dissolves cellular membranes without disturbing protein–protein interactions. Triton is usually used at 0.1% in PBS at room temperature for 10 minutes for permeabilization. Besides cell membrane permeabilization, this detergent will partially dissolve the nuclear membranes, making them suitable for nuclear staining also. These fixed cells were analyzed for fluorescence emission by using standard filter sets, but with a DAPI filter with excitation/emission wave-

lengths of 358/400 nm using a fluorescent microscope (Zeiss). The cells showed decreased fluorescence and less response in higher basic medium. Hence the **BPPIH** compound was internalized into both cytoplasm and nucleus.

Anion recognition studies

To study the application of these two organic sensor molecules as selective anion sensors, **BPPIH** and **BPBIH** are tested with different guest anions and the results obtained (Fig. S28 and S29, ESI†) clearly show their selective affinity towards F⁻. The interference study of **BPPIH** with other anions is shown in Fig. S42.† However, comparative studies reflect that **BPBIH** is more sensitive towards F⁻ although colorimetric responses for **BPPIH** are more promising. The pH changes during titration of **BPPIH** and **BPBIH** with increasing level of fluoride addition from 0–2.0 eq. are shown in Fig. 6a and c.

In the case of **BPPIH** the absorbance peak at 265 nm gradually increases in intensity with the appearance of a new peak at 340 nm which also simultaneously increases in intensity. The color turns from colorless to yellow (Fig. 6a). With time an interesting observation is noticed. The peak at 340 nm starts to diminish gradually with the generation of a new peak at 465 nm (Fig. 6b). The color turns to deep red. In fluorescence, the peak at 365 nm diminishes in intensity after TBAF addition with little or no bathochromic shift (Fig. S30, ESI†). For **BPBIH** before addition of F⁻, the initial absorbance peak at 295 nm reduces and two new peaks are generated in the higher wavelength region at ~325 and 395 nm (Fig. 6c).

While studying the emission responses it is found that this molecule is a ratiometric sensor for F⁻. The peak at 380 nm
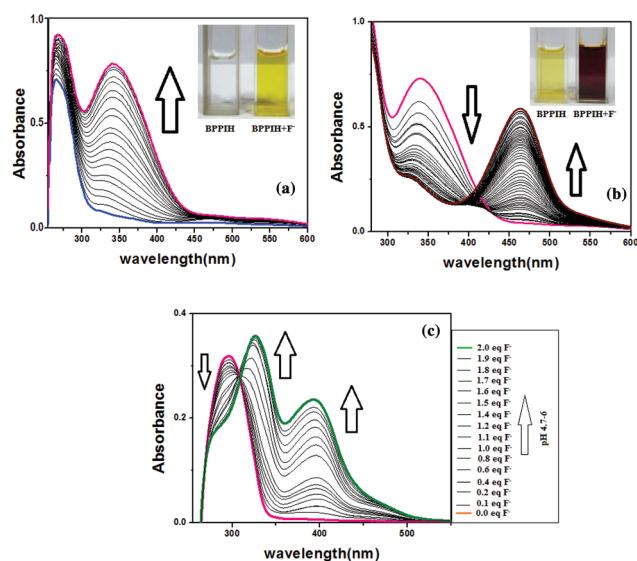

Fig. 6 (a) UV-Vis titration curve of **BPPIH** (1 × 10⁻⁵ M) with TBAF (0–2.0 eq.); inset: color change of **BPPIH** from colorless to yellow with TBAF; pH changes from 5.0–11.0; (b) UV changes of **BPPIH** after one time addition of 2 equivalents of TBAF within a time interval of 1 h; inset: color change of **BPPIH** from yellow to reddish with TBAF; (c) UV-Vis titration of **BPBIH** (1 × 10⁻⁵ M) with TBAF (0–2.0 eq.); inset: color change of **BPBIH** from yellow to reddish with TBAF; pH changes from 4.7–6.0.

This journal is © The Royal Society of Chemistry and Owner Societies 2017

Photochem. Photobiol. Sci., 2017, **16**, 1654–1663 | **1659**

reduces in intensity after addition of TBAF and simultaneously a new peak at 440 nm is developed with increasing intensity having an isosbestic point at 420 nm (Fig. S31, ESI†). Thus **BPBIH** shows ratiometric responses with F⁻ both in absorbance and emission profiles. However **BPPIH** shows a ratiometric approach only in its absorption profile. PET is the cause of quenching of photoluminescence in the case of **BPPIH** while PET followed by ICT is the reason for quenching and then shifting (bathochromic) for **BPBIH**. The degree of quenching in the emission intensity of the sensors with TBAF is depicted in (Fig. S32, ESI†) where the quenching is in the following order of **BPBIH** > **BPPIH**.

The job's plot shows a 1 : 1 ratio for both **BPPIH** and **BPBIH** (Fig. S33 and S34, ESI†). On calculating the binding constant values for the two sensors with F⁻ with the help of Benesi–Hildebrand equation it is found that the binding of F⁻ with them is in the order of **BPPIH** > **BPBIH**. The values are 0.88×10^5 M⁻¹ and 0.109×10^5 M⁻¹, respectively (Fig. S35 and S36, ESI†).

Since ratiometric sensors have added advantages over non ratiometric sensors due to influence of the latter by several environmental factors, excitation, concentration[7] *etc*. **BPBIH** is a more promising F⁻ sensor compared to **BPPIH**, although the binding constant values are in the reverse order. The presence of two covalently linked chromogenic centres in **BPBIH** in comparison to **BPPIH** may be the reason for this difference.

LOD turns out to be 6.2×10^{-5} M for **BPPIH** and 2.5×10^{-5} M for **BPBIH** (Fig. S37 and S38, ESI†). **BPPIH** shows a feeble response for acetate too (Fig. S28, ESI†).

NMR study

To gain further insights into the binding processes ¹H-NMR titrations are performed (Fig. 7 and Fig. S41, ESI†). The NH proton assigned as 'b' (Scheme 1) appears at a more downfield position (~10.89 ppm) and is therefore more acidic as compared to the NH proton assigned 'a' (~8.3 ppm). Löwdin atomic charges from DFT calculations for the NH atoms of the geometry optimized structure are found to support the NMR results. The charges on the four hydrogen atoms are 37 H: 0.32 (NH_a), 38 H: 0.33 (NH_b), 43 H: 0.33 (NH_b), and 44 H: 0.32 (NH_a) (Fig. S39, ESI†), respectively. It was reflected from theoretical calculations that the charge densities on the amide NH_b protons are more than those on the NH_a protons attached
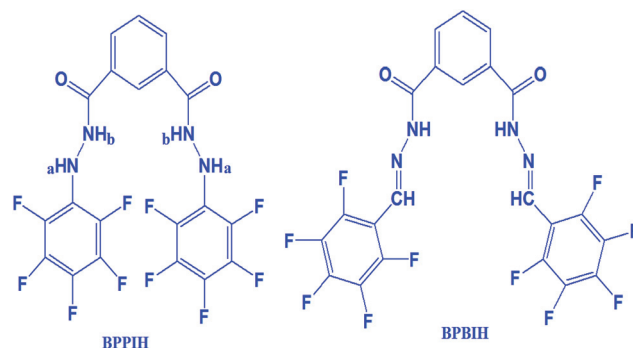
Scheme 1

to the benzene ring as shown above. Hence quite naturally the NH_b protons are more acidic compared to the NH_a protons, which is further confirmed when we performed the NMR titration experiments with TBAF. The NH_b protons disappear first at 0.2 eq. addition of F⁻ followed by the NH_a (at 8.3 ppm) which disappears at 0.4 eq. of F⁻ addition. There is no shifting of peak positions, confirming the presence of strong H-bonding interaction with the incoming F⁻ ion.[1c] In case of **BPBIH** the NH protons appear at 12.5 ppm and the CH protons (azomethine) at 10.79 ppm. From theoretical calculations on the molecule it was found that the atomic charges on the NH protons were 0.33 for H39 and 0.33 for H44 (Fig. S40, ESI†), which are comparatively higher than the NH_b protons of **BPPIH** showing their more acidic nature than the former. Titration with TBAF makes the NH protons disappear at about 0.4 eq. addition of the salt while the C/H protons undergo upfield shifting with complete flattening at 0.4 eq. of the anion addition. The aromatic protons also undergo upfield shifting indicating acid–base pathway (*i.e.* proton abstraction).[1b] On further addition of 1 equiv. of F⁻ at 16.1 ppm a clear triplet response confirms the formation of HF₂⁻ as a result of proton abstraction (Fig. S41, ESI†).

Energy minimized structures of BPPIH and BPBIH with their F⁻ adducts

Ab initio calculations were done in Turbomole (v7.0) to investigate the structural changes of **BPPIH** and **BPBIH** upon their complexation with F⁻ (Tables S11–S14†). Density functional theory calculations employing the BP86 correlation function and using the def SV (P) basis set were performed. In the case of **BPPIH**: F⁻ (1 : 1) adduct formation the N–H distances of N17, N18, N8, N7 all become elongated on F⁻ interaction (the respective NH distances of the host molecule are mentioned here 0.84, 0.87, 0.87 and 0.90 Å). In **BPPIH**: 2F⁻ (1 : 2) adduct F⁻ interacts more with the outward facing N–H hydrogen of N17 and N7 with the distances elongating to 1.12 and 1.08 Å respectively (Fig. 8a). The distances between F⁻ and H atoms in both the cases are approximately between 1.3 and 1.4 Å, which suggests strong H-bonding between **BPPIH** and F⁻. In the case of **BPBIH** : F⁻ (1 : 1) adduct formation the N–H distances of N17 and N8 atoms have been found to elongate to
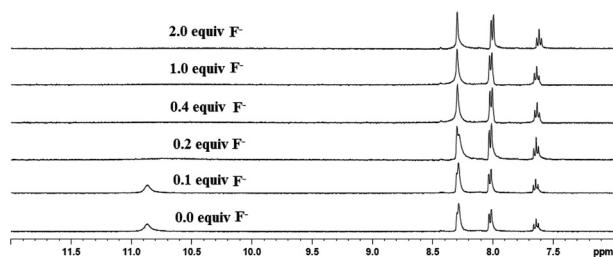

Fig. 7 ¹H-NMR titration of **BPPIH** (1×10^{-3} M) with TBAF (0–2 eq.) in DMSO-d⁶.
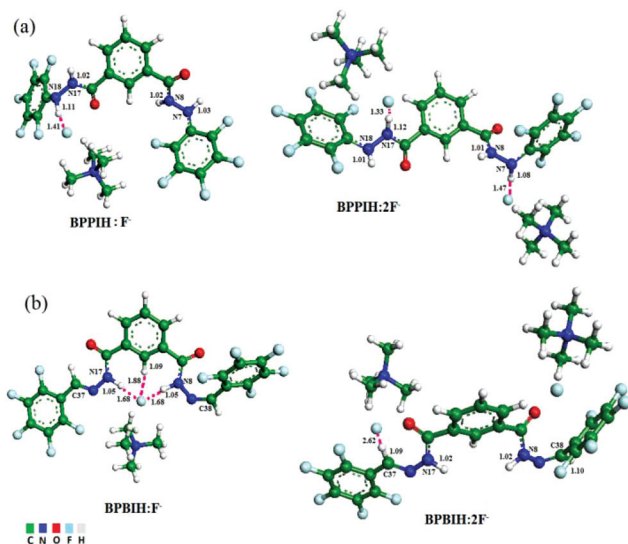
Fig. 8 (a) Geometry optimized structure of **BPPIH** with F$^-$ and (b) geometry optimized structure of **BPBIH** with F$^-$.

1.05 and 1.05 Å from 1.01 and 1.02 Å respectively. The H⋯F$^-$ distances 1.68 Å in both cases suggest H-bonding interaction. However, further addition of F$^-$ doesn't reflect any subtle changes in the network (Fig. 8b).

The interaction energy results as shown in Table 2 are as expected and in support of the experimental results where **BPPIH** is a better fluoride sensor than **BPBIH** and A is the sensor **BPPIH/BPBIH** and B is NMe$_4$F. The interaction energy of **BPPIH** with F$^-$ is less positive than that of **BPBIH** with F$^-$, which suggests that interaction of **BPPIH** with F$^-$ is more favourable than that of **BPBIH** with F$^-$.

Furthermore, in line with host⋯guest interactive studies, between **BPPIH**⋯F$^-$/**BPPIH**⋯2F$^-$ and **BPBIH**⋯F$^-$/**BPBIH**⋯2F$^-$, as reflected from DFT-D3 studies, the **BPPIH**⋯2F$^-$ and **BPBIH**⋯2F$^-$ energy orders are the minimum with regard to **BPPIH**⋯F$^-$ and **BPBIH**⋯F$^-$ interactive mode, hence taking their relative energy values to be null and void the relative energy of **BPPIH**: F$^-$ and **BPBIH**⋯F$^-$ is found to be 327.32 E_h and 327.83 E_h respectively.

Future scope

Interfacing of the pH sensor (BPPIH) with suitable circuitry. The pH sensor (**BPPIH**)[27] invention can be further interfaced

Table 2 Interaction energy between sensor⋯F$^-$

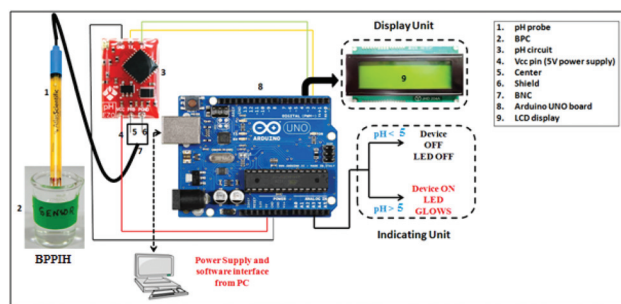| Sensor⋯F$^-$ interaction	$E_{(A,B)}$ (in E_h)	$E_{(A)}$ (in E_h)	$E_{(B)}$ (in E_h)	$\Delta E_{int} = E_{(A,B)} - [E_{(A)} + E_{(B)}]$ (in E_h)
Sensor⋯F$^-$ interaction (1:1)				
BPPIH⋯F$^-$	−2433.80	−2133.22	−784.74	484.16
BPBIH⋯F$^-$	−2509.44	−2209.38	−784.74	484.68
Sensor⋯F$^-$ interaction (1:2)				
BPPIH⋯F$^-$	−2761.12	−2133.22	−1569.48	941.58
BPBIH⋯F$^-$	−2837.268	−2209.38	−1569.48	941.59

Fig. 9 Interfacing of **BPPIH** with suitable circuitry.

with suitable circuitry interfaced with desired programming for enhanced practical applications (Fig. 9). A recommended device would be a micro footprint pH monitoring subsystem (pH circuit, Atlas Scientific) that might be connected to the device for fetching the pH related data of solutions that keep on swinging between particular pH ranges. The final output would be fed to a functional pin of Arduino UNO in order to interpret the pH measures as digital outputs indicated by ON and OFF signs of LEDs and suitable display mechanisms.

Conclusions

In conclusion we have synthesized two novel pH and F$^-$ sensors, **BPPIH** and **BPBIH**; the former showcases high emission intensity in protic media due to greater rigidity in its structure than that in the latter (having lower intensity) due to a higher order of flexibility. The four NH protons in **BPPIH** make the molecule a very useful pH sensor in the pH range 5.0–10.0. The sensor was applied to monitor pH changes inside Human cervical carcinoma cell lines (HeLa). In addition both the sensors showed selective affinity towards the F$^-$ anion. Between the two, **BPBIH** turned out to be a ratiometric F$^-$ sensor with a lower limit of F$^-$ detection than **BPPIH**. The experimental findings were all well supported by Density Functional Theory (DFT) and modern DFT-D3 calculations. In addition the pH sensor **BPPIH** can be further interfaced with suitable circuitry interfaced with desired programming for ease of access and enhancement of practical applications. This easy to prepare, promising sensor opens a new horizon to synthesize similar sensor molecules having improved multi ion sensing ability.

Conflicts of interest

There are no conflicts of interest to declare.

Acknowledgements

This journal is © The Royal Society of Chemistry and Owner Societies 2017

Photochem. Photobiol. Sci., 2017, **16**, 1654–1663 | **1661**

Notes and references

1 (a) D. Saravanakumar, S. Devaraj, S. Iyyampillai, K. Mohandoss and M. Kandaswamy, *Tetrahedron Lett.*, 2008, **49**, 127; (b) M. Kumar, R. Kumar and V. Bhalla, *Chem. Commun.*, 2009, 7384; (c) M. Kumar, N. Kumar, V. Bhalla, H. Singh, P. R. Sharma and T. Kaur, *Org. Lett.*, 2011, **13**, 1422; (d) P. Ghosh, B. G. Roy, N. C. Murmu and P. Banerjee, *RSC Adv.*, 2015, **5**, 27387; (e) J. N. Babu, V. Bhalla, M. Kumar, R. K. Mahajan and R. K. Puri, *Tetrahedron Lett.*, 2008, **49**, 2772; (f) V. Bhalla, R. Kumar, M. Kumar and A. Dhir, *Tetrahedron*, 2007, **63**, 11153; (g) V. Bhalla, A. Gupta, M. Kumar, D. S. S. Rao and S. K. Prasad, *ACS Appl. Mater. Interfaces*, 2013, **5**, 672; (h) M. Kumar, R. Kumar and V. Bhalla, *Tetrahedron Lett.*, 2010, **51**, 5559; (i) V. Bhalla and M. Kumar, *Dalton Trans.*, 2013, **42**, 13390; (j) A. Roy Chowdhury, P. Ghosh, B. G. Roy, S. K. Mukhopadhyay, N. C. Murmu and P. Banerjee, *Sens. Actuators, B*, 2015, **220**, 347; (k) A. Roy Chowdhury, P. Ghosh, B. G. Roy, S. K. Mukhopadhyay, P. Mitra and P. Banerjee, *RSC Adv.*, 2015, **5**, 62017; (l) P. Ghosh, N. Kumar, S. K. Mukhopadhyay and P. Banerjee, *Sens. Actuators, B*, 2016, **224**, 899; (m) P. Ghosh, B. G. Roy, S. Jana, S. K. Mukhopadhyay and P. Banerjee, *Phys. Chem. Chem. Phys.*, 2015, **17**, 20288; (n) P. Ghosh and P. Banerjee, *Phys. Chem. Chem. Phys.*, 2016, **18**, 22805; (o) P. Ghosh and P. Banerjee, *Chem. Phys.*, 2016, **478**, 103; (p) M. Kumar, R. Kumar and V. Bhalla, *RSC Adv.*, 2011, **1**, 1045; (q) M. Kumar, R. Kumar and V. Bhalla, *Tetrahedron Lett.*, 2013, **54**, 1524; (r) V. Bhalla, R. Tejpal and M. Kumar, *Tetrahedron*, 2011, **67**, 1266.

2 (a) V. Snitsarev, M. N. Young, R. M. S. Miller and D. P. Rotella, *PLoS One*, 2013, **8**, 79834; (b) M. Homocianu, A. Airinei and D. OrtansaDorohoi, *J. Adv. Res. Phys.*, 2011, **2**, 011105; (c) M. A. Haidekker, T. P. Brady, D. Lichlyter and E. A. Theodorakis, *Bioorg. Chem.*, 2005, **33**, 415; (d) T. S. Kotsyuba, V. M. Granchak, I. I. Dilung and V. P. Kondilenko, *Theor. Exp. Chem.*, 1997, **33**, 34; (e) Z. Yang, J. Cao, Y. He, J. H. Yang, T. Kim, X. Peng and J. S. Kim, *Chem. Soc. Rev.*, 2014, **43**, 4563; (f) *Handbook of Fluorescence Spectroscopy and Imaging*, M. Sauer, J. Hofkens and J. Enderlein, WILEY-VCH Verlag GmbH & Co. KGaA, Weinheim, Copyright 2011, ISBN: 978-3-527-31669-4.

3 (a) https://drtijanadc.wordpress.com/2012/07/02/the-essentials-of-ph/; (b) http://www.lifewithgreens.com/ph-and-your-health; (c) http://www.mindbodygreen.com/0-3400/What-You-Need-to-Know-About-pH.html; (d) http://www.google.co.in/patents/WO2004016297A1.

4 (a) F. Doria, M. Folini, V. Grande, G. Cimino-Reale, N. Zaffaronib and M. Freccero, *Org. Biomol. Chem.*, 2015, **13**, 570; (b) Y. Nia and J. Wu, *Org. Biomol. Chem.*, 2014, **12**, 3774; (c) C. Y. Ang, S. Y. Tan and Y. Zhao, *Org. Biomol. Chem.*, 2014, **12**, 4776.

5 P. Ghosh, A. Roy Chowdhury, S. K. Saha, M. Ghosh, M. Pal, N. C. Murmu and P. Banerjee, *Inorg. Chim. Acta*, 2015, **429**, 99.

6 (a) P. Ghosh, B. G. Roy, S. Jana, S. K. Mukhopadhyay and P. Banerjee, *Phys. Chem. Chem. Phys.*, 2015, **17**, 20288; (b) P. Banerjee, S. Sproules, T. Weyhermuller, S. D. George and K. Wieghardt, *Inorg. Chem.*, 2009, **48**, 5829S; (c) R. Presow, M. Ghosh, E. Bill, T. Weyhermüller and K. Wieghardt, *Inorg. Chim. Acta*, 2011, **374**, 226.

7 A. Roy Chowdhury, P. Ghosh, S. K. Saha, P. Mitra and P. Banerjee, *Spectrochim. Acta, Part A*, 2014, **124**, 492.

8 (a) M. Sarkar, R. Yellampalli, B. Bhattacharya, R. K. Kanaparthi and A. Samanta, *J. Chem. Sci.*, 2007, **119**, 91; (b) Y. Kubo, M. Yamamoto, M. Ikeda, M. Takeuchi, S. Shinkai, S. Yamaguchi and K. Tamao, *Angew. Chem., Int. Ed.*, 2003, **42**, 2036.

9 (a) F. Neese, *2.6, reVision 4 ed.*, ed. M.-P. I. f. B. Chemie, Mulheim/Ruhr, Germany, 2005; (b) http: //www.cosmologic. de/files/downloads/manuals/TURBOMOLE-Users-Manual_ 70.pdf; (c) S. Grimme, J. Antony, S. Ehrlich and H. Krieg, *J. Chem. Phys.*, 2010, **132**, 154104; (d) S. Grimme, S. Ehrlich and L. Goerigk, *J. Comput. Chem.*, 2011, **32**, 1456.

10 A. D. Becke, *J. Chem. Phys.*, 1986, **84**, 4524.

11 A. D. Becke, *J. Chem. Phys.*, 1993, **98**, 5648.

12 C. T. Lee, W. T. Yang and R. G. Parr, *Phys. Rev. B: Condens. Matter*, 1988, **37**, 785.

13 A. Schafer, H. Horn and R. J. Ahlrichs, *Chem. Phys.*, 1992, **97**, 2571.

14 A. Schafer, C. Huber and R. J. Ahlrichs, *Chem. Phys.*, 1994, **100**, 5829.

15 F. J. Neese, *Phys. Chem. Solids*, 2004, **65**, 781.

16 *ShelXTL, v 6.14*, Bruker AXS Inc., Madison, WI, 2003.

17 (a) P. Banerjee, G. Mostafa, A. Castineiras and S. Goswami, *Eur. J. Inorg. Chem.*, 2007, **2007**, 412; (b) P. Ghosh, A. Roy Chowdhury, S. K. Saha, M. Ghosh, M. Pal, N. C. Murmu and P. Banerjee, *Inorg. Chim. Acta*, 2015, **429**, 99; (c) P. Ghosh, A. Roy Chowdhury, M. Corbella, A. Bhaumik, P. Mitra, S. M. Mobin, A. Mukherjee, S. Basu and P. Banerjee, *Dalton Trans.*, 2014, **43**, 13500.

18 G. Lever, D. J. Cole, N. D. M. Hine, P. D. Haynes and M. C. Payne, *J. Phys.: Condens. Matter*, 2013, **25**, 152101.

19 (a) M. Levitus, G. Zepeda, H. Dang, C. Godinez, T. A. V. Khuong, K. Schmieder and M. A. Garcia-Garibay, *J. Org. Chem.*, 2001, **66**, 3188; (b) D. T. McQuade, J. Kim and T. M. Swager, *J. Am. Chem. Soc.*, 2000, **122**, 5885; (c) K. A. Walters, K. D. Ley and K. S. Schanze, *Langmuir*, 1999, **15**, 5676; (d) C. Weder and M. S. Wrighton, *Macromolecules*, 1996, **29**, 5157.

20 G. R. Kumar and P. Thilagar, *Dalton Trans.*, 2014, **43**, 7200.

21 (a) P. Suppan, *Spectrochim. Acta, Part A*, 1973, **30A**, 1939; (b) C. S. Oliveira, K. P. Branco, M. S. Baptista and G. L. Indig, *Spectrochim. Acta, Part A*, 2002, **58**, 2971;

(*c*) Y. Jung and J. Hwang, 2013 Optical Society of America; OCIS codes: 300.6340, 300.1030.

22 (*a*) S. A. McFarland and N. S. Finney, *J. Am. Chem. Soc.*, 2001, **123**, 1260; (*b*) I. Berlman, *Handbook of Fluorescence Spectra of Aromatic Molecules*, Academic Press, New York, 1971; (*c*) N. I. Nizhegorodov and W. S. Downey, *J. Phys. Chem.*, 1994, **98**, 5639 and references therein.

23 D. Cui, X. Qian, F. Liu and R. Zhang, *Org. Lett.*, 2004, **6**(16), 2757.

24 V. V. Shynkar, A. S. Klymchenko, E. Piémont, A. P. Demchenko and Y. Mély, *J. Phys. Chem. A*, 2004, **108**, 8151.

25 J. Han and K. Burgess, *Chem. Rev.*, 2010, **110**(5), 2709.

26 (*a*) R. Wang, Y. Chunwei, F. Yu and L. Chen, *Trends Anal. Chem.*, 2010, **29**(9), 1005; (*b*) M. H. Lee, J. H. Han, J. H. Lee, N. Park, R. Kumar, C. Kang and J. S. Kim, *Angew. Chem., Int. Ed.*, 2013, **52**, 6206; (*c*) G. Despras, A. I. Zamaleeva, L. Dardevet, C. Tisseyre, J. G. Magalhaes, C. Garner, M. D. Waard, S. Amigorena, A. Feltz, J. M. Malleta and M. Collot, *Chem. Sci.*, 2015, **6**, 5928; (*d*) B. Shia, Y. Sua, L. Zhanga, R. Liua, M. Huanga and S. Zhaoa, *Biosens. Bioelectron.*, 2016, **82**, 233; (*e*) X.-D. Liu, Y. Xu, R. Sun, Y.-J. Xu, J.-M. Lu and J.-F. Ge, *Analyst*, 2013, **138**, 6542; (*f*) Y. Xu, Y. Liu and X. Qian, *J. Photochem. Photobiol., A*, 2007, **190**, 1; (*g*) P. T. Snee, R. C. Somers, G. Nair, J. P. Zimmer, M. G. Bawendi and D. G. Nocera, *J. Am. Chem. Soc.*, 2006, **128**(41), 13320.

27 A. Roy Chowdhury, P. Ghosh, S. Paul, S. Bhuyan, J. C. Bose K, S. Mukhopadhyay and P. Banerjee, *Anal. Methods*, 2017, **9**, 124.

This journal is © The Royal Society of Chemistry and Owner Societies 2017

Photochem. Photobiol. Sci., 2017, **16**, 1654–1663 | **1663**